# Pattern formation of chevrons in the conduction regime in homeotropically aligned liquid crystals


doi: 10.1103/PhysRevE.61.2769

# Pattern formation of chevrons in the conduction regime in homeotropically aligned liquid crystals

Jong-Hoon Huh,[1] Yoshiki Hidaka,[1] Axel G. Rossberg,[2] and Shoichi Kai[1]
[1]*Department of Applied Physics, Faculty of Engineering, Kyushu University, Fukuoka 812-8581, Japan*
[2]*Department of Physics, Kyoto University, Kyoto 606-8502, Japan*
(Received 24 May 1999)

We report on chevrons (herringbonelike patterns) observed in *homeotropically* aligned liquid crystals with high electric conductivity. We focus our attention on two types of chevrons observed in the *conduction* regime. The threshold voltage and the characteristic double periodicity of chevrons (i.e., the short wavelength $\lambda_1$ of the striated rolls and the long wavelength $\lambda_2$ of the chevron bands) have been measured as functions of the applied electric frequency $f$. With the aid of a crossed polarizer set, we have, in addition, determined the director field which shows a periodic in-plane rotation for our chevrons (with a wavelength $\lambda_2$). We arrived at the types of chevrons after qualitatively different bifurcation sequences with increasing voltage. The frequency dependence of $\lambda_2$ also shows a qualitatively different behavior with respect to the two types of chevrons. The experimental results are discussed in terms of recent theoretical investigations.

PACS number(s): 61.30.−v, 47.20.Lz, 47.20.Ky, 47.65.+a

## I. INTRODUCTION

Pattern formation in dissipative systems driven out far from equilibrium is common in nature. There are many examples in fluid physics, chemistry, biology, and in many other fields (see, e.g., Ref. [1]). Due to the progress of theoretical and numerical research, the universal aspects of the various patterns in fluid systems are now well understood at least near the primary instability [1,2]. The present work addresses electroconvection (EC) in nematic liquid crystals (nematics), which has been intensively studied in the last decades (see, e.g., Refs. [3–8]). EC provides a rich variety of pattern-formation phenomena, and has become a main paradigm for anisotropic dissipative structures.

When one applies an alternating electric field $\mathbf{E}=E(f)\hat{\mathbf{z}}$ with $E(f)=E_0\cos(2\pi ft)$ across a thin nematic slab (of thickness $d=10-100\ \mu$m) between two electrode plates, one observes typically striped (roll) patterns in the $xy$ plane. The basic mechanism of EC is well understood in terms of the Carr-Helfrich effect due to anisotropic properties of liquid crystals [9,10]. In addition to the flow field of the convection rolls, the director $\mathbf{n}=(n_x,n_y,n_z)(\mathbf{n}^2=1,\mathbf{n}\equiv-\mathbf{n})$, which is defined as the locally averaged orientation of the rodlike molecules of nematics [11,12], plays an important role in the pattern formation process.

The essential features can easily be demonstrated in the planar geometry [described by $\mathbf{n}_0=(1,0,0)$ for the initial state] [3,4,11]. Any director fluctuation out of the horizontal plane ($n_z\neq0$) leads to an inhomogeneous charge distribution due to the electric conduction anisotropy of the nematics ($\sigma_a\neq0$). If the resulting Coulomb force above a critical voltage $V_c$ overcomes the viscous force, a material flow is induced. This flow in turn gives rise to a torque on the director, by which the fluctuations of the director are reinforced. Consequently, an electrohydrodynamic instability is induced which leads to the convection patterns. The details of the patterns depend on frequency $f$. At low frequencies, the charge relaxation time $\tau_\sigma$ is much shorter than the period $f^{-1}$ of the low frequency electric field $E(f)(\tau_\sigma f\ll1)$, while the director relaxation time $\tau_d$ is much larger than $f^{-1}(\tau_d f\gg1)$. Therefore, in this so-called *conduction* regime the director cannot follow the external field $E(f)$, and remains stationary to leading order. In the dielectric regime ($f>f_c$), above a certain cutoff frequency $f_c=O(\tau_\sigma^{-1})$, on the other hand, $\tau_\sigma$ becomes larger than $f^{-1}(\tau_\sigma f\gg1)$, and charges cannot accumulate. The director oscillates in phase with the alternating field $E(f)$, while the charge distribution is stationary.

One also has to consider two different orientations of the rolls. In the normal-roll case the wave vector $\mathbf{q}$ is parallel to the preferred direction ($\hat{\mathbf{x}}$). But the chiral symmetry can also be broken in the oblique-roll case with a finite angle between $\mathbf{q}$ and $\hat{\mathbf{x}}$. There exist two equivalent variants of such oblique rolls, zig (positive angle) and zag (negative angle). Oblique rolls appear typically very near to threshold by a secondary bifurcation, but in some case even directly at the convective threshold for low frequency. Then there exists a Lifshitz frequency $f_L$ which separates the oblique rolls ($f<f_L$) from the normal ones ($f>f_L$). In the dielectric regime the primary bifurcation is to normal rolls, but very near to threshold a bifurcation to the chevron patterns takes place. They consist of alternating stripes of zig and zag rolls with a very small wavelength ($\lambda_1\ll d$), where the width of the stripes ($\lambda_2$) is much larger than $\lambda_1$.

Very recently it has become clear that there exists a new type of symmetry-breaking bifurcation toward abnormal rolls with increasing voltage [13,14]. Abnormal rolls are characterized by a homogeneous rotation of the **C** director (i.e., the projection of the director **n** onto the $xy$ plane). Unlike the normal rolls at threshold, the **C** director is not parallel to **q** for abnormal rolls. The bifurcation can be understood by the tendency of the director to escape a high-viscosity configuration by rotating out of the shear plane [13,14].

Recently, EC in the *homeotropic* geometry [described by $\mathbf{n}_0=(0,0,1)$ for the initial state] has attracted much atten-

 

tion [15–23]. In the homeotropic case, the basic state is isotropic in the $xy$ plane. Above a certain characteristic voltage $V_F$[$\sim$4 V for *p*-methoxybenzilidene-*p'*-*n*-butylaniline (MBBA)] the continuous rotational symmetry is spontaneously broken by the Fréedericksz transition, where the director tilts off the $z$ axis. The projection of the director on the $xy$ plane (the **C** director) can be spontaneously chosen. Consequently, there must exist a soft mode, the so-called Goldstone mode, which corresponds to a slowly varying azimuthal rotation of the director. The important point is that this Goldstone mode can easily couple to the convective mode. We have already reported on a drastic role of the Goldstone mode for pattern formation and dynamics in EC [18–20]. For finite magnetic fields ($\mathbf{H}\|\hat{\mathbf{x}}$) the convection phenomena in the homeotropic system are quite similar to the planar case, since the Fréedericksz transition leads to a planar configuration with a preferred orientation ($\hat{\mathbf{x}}$) in the central part of the sample. There exists always an abnormal-roll bifurcation [22,23]. Only very recently have chevrons in the *conduction* regime also been observed in the homeotropic system [21,22].

Until now, almost all studies of chevrons have been performed in the planar system (see, e.g., Refs. [3,4,24–31]) and only very few exist in the homeotropic case [32,33]. Moreover, almost studies of chevrons in both planar and homeotropic systems focused on conventional chevrons in the dielectric regime ($f>f_c$). Previous studies were mainly devoted to the question of how the threshold and wavelength of striated zig and zag rolls depend on the applied frequency $f$, the sample thickness, electric conductivities, the dielectric constant, or the magnitude of the stabilizing magnetic field (see, e.g., Refs. [3,4,25,27,32,34–36]). However, the underlying mechanism for chevron structure is still not too well understood.

In the present paper we focus on chevrons in the *conduction* regime for the *homeotropic* system by varying the electric conductivity for the nematics. In the case of low conductivity, only one type of chevron [the defect-mediated chevron (DMC)] has been observed. It is characterized by spatially periodic defect lines between alternating zig and zag rolls. On the other hand, in the case of high conductivity, in addition to the DMC we have observed another type of chevron, which we will call the defect-free chevron (DFC). The past classification of chevrons [34,37] was done only through the difference of their wavelengths $\lambda_1$ of the striated rolls, that is, CV-A, $\lambda_1\sim d$, and CV-B, $\lambda_1\ll d$; typically, $\lambda_1\sim d/20-d/10$. However, this classification does not describe their morphology and properties well, because of the rich variety of chevrons.

In the homeotropic case, the DFC is better characterized by alternating zig and zag rolls without defects, while the DMC shows a herringbone structure with defect lines. We have investigated pattern formation of the two types of chevrons in highly conductive samples. The DMC and DFC in this study have been observed below and above a certain characteristic frequency $f_w(f_w<f_c)$, respectively. With the aid of a weak magnetic field (stabilizing the director) and a crossed polarizer set, we have observed a generic bifurcation sequence for $f<f_w$ (normal rolls $\rightarrow$ abnormal rolls $\rightarrow$ defect chaos $\rightarrow$ DMC) with increasing voltage. For $f>f_w$, on the other hand, we have observed that the DFC typically shows a bifurcation sequence (Fréedericksz transition $\rightarrow$ prewavy pattern $\rightarrow$ DFC) with increasing voltage.

In addition, we have investigated in detail the double periodicity (two characteristic wavelengths $\lambda_1$ and $\lambda_2$) of the two types of chevrons as functions of the frequency $f$. With the aid of a crossed polarizer set, we have mapped a periodic **C**-director structure for the DMC and DFC in the $xy$ plane. On the basis of the experimental results, we discuss the underlying mechanisms for the DMC and DFC and compare with recent theoretical findings [38–40].

## II. RESULTS AND DISCUSSION

### A. Experimental preparation

A nematic liquid crystal MBBA was used, which was filled between two parallel glass plates whose surfaces were coated with transparent electrodes (indium tin oxide). The gap width $d=50$ $\mu$m between the two electrodes was maintained with polymer spacer. The lateral size of the sample was $1\times1$ cm$^2$. We achieved the standard homeotropic geometry by treating the two electrodes with a surfactant DMOAP (*n*-*n'*-dimethyl-*n*-octadecyl-3-aminopropyl-trimethoxysilyl chloride). We prepared three samples of which electric conductivities were varied ($\sigma_\parallel=7.49\times10^{-9}$–$9.08\times10^{-7}$ $\Omega^{-1}$ m$^{-1}$) to be controlled by doping of TBAB (tetra-*n*-butyle-ammonium bromide). Their dielectric anisotropies $\epsilon_a$ were slightly different in range from $-0.34$ to $-0.25$ due to the treatment. The temperature of the sample in Teflon-wrapped copper cavity was stabilized at 30 $\pm0.1$°C by an electric control system (Digital Controller DB500). An alternating electric field $E$ with a frequency $f$ was applied across the thin sample [$\mathbf{E}=(0,0,\pm E_z)$], and a constant magnetic field (an electromagnet, TAMAGAWA TM-WTV8615C) was set parallel to the glass plates [$\mathbf{H}=(H_x,0,0)$]. In order to monitor the **C** director, we used a crossed polarizer set which could be rotated around the $z$ axis or removed readily. The patterns were observed in the $xy$ plane by use of a charge-coupled-device camera (SONY XC-75) mounted on a microscope.

### B. Results

We have measured the threshold $V_c(f)$ for the onset of pattern formation with respect to various electric conductivities, as shown in Fig. 1. The threshold $V_c(f)$ of sample 1 with low conductivity shows a well-known frequency dependence (see, e.g., Refs. [11,41]). The cutoff frequency $f_c$ moves to a higher frequency with increasing conductivity. In the dielectric regime ($f>f_c$), conventional chevrons with a small wavelength $\lambda$ of striated rolls ($\lambda\ll d$) were observed, similarly to those of the planar system [29], on which we will not focus in the present paper. The cutoff frequency $f_c$ in samples 2 and 3 with high conductivities have not been measured, in order to avoid damaging the cells due to the required high voltages.

Now let us consider chevrons in the conduction regime ($f<f_c$). Two types of chevrons were observed below and above a certain characteristic frequency $f_w(<f_c)$ in samples 2 and 3. On the other hand, only one type of chevron was observed in sample 1, because the other type of chevron was replaced by the dielectric mode (see Refs. [11,29,42]). In the

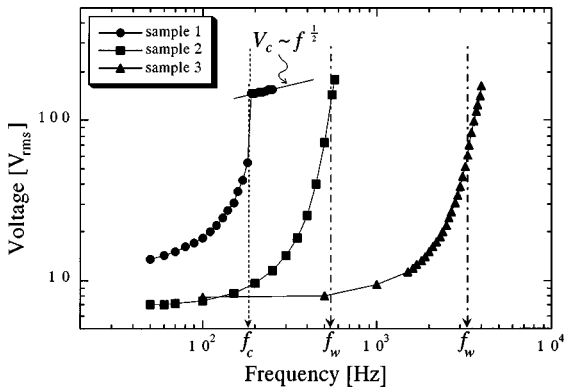


FIG. 1. Threshold $V_c$ of onset of pattern formation on three samples ($d=50$ $\mu$m) with various electric conductivities. The threshold voltages were determined by observing the corresponding patterns with no polarizer. Sample 1: $\sigma_\parallel=7.49\times10^{-9}$ $\Omega^{-1}$ m$^{-1}$ and $\epsilon_a=-0.34$. Sample 2: $\sigma_\parallel=6.25\times10^{-8}$ $\Omega^{-1}$ m$^{-1}$ and $\epsilon_a=-0.25$. Sample 3: $\sigma_\parallel=9.08\times10^{-7}$ $\Omega^{-1}$ m$^{-1}$ and $\epsilon_a=-0.29$. $f_c$ for sample 1 represents the cutoff frequency that separates the conduction regime from the dielectric one. $f_w$ represents another characteristic frequency in the conduction regime. See text for details. Hereafter, all the observations and measurements except Fig. 8 have been performed on sample 3.

range $f_w<f<f_c$ of sample 3 ($f_w\simeq3150$ Hz), a typical chevron pattern for the homeotropic system is shown in Fig. 2. At a voltage $V=149.40$ V ($V_c=140.54$ V at $f=3900$ Hz), when starting from the homogeneous Fréedericksz state (the threshold $V_F\simeq3.92$ V), a well ordered chevron pattern was observed, as shown in Fig. 2(a). Thereafter we call the chevron pattern in Fig. 2(a) a DFC, which is characterized by stripes with alternating zig and zag rolls. Figure 2(a) is equivalent to chevrons formed via the Williams domains at $f_w<f<f_c$ in the planar case with high conductivity [29]. A DFC would change into a spatiotemporally chaotic state with time, as shown in Fig. 2(b). Note, however, that locally regular chevron structures are still visible in Fig. 2(b). Such a pattern dynamics is very similar to that of the soft-mode turbulence (see Fig. 1 of Ref. [19]) which suggests a coupling between the Goldstone mode and convection rolls, as mentioned in Sec. I [18,19].

For $f<f_w$, on the other hand, we have observed the other type of chevron at $V=15.82$ V ($V_c=15.08$ V at $f=2000$ Hz) as shown in Fig. 3(a). Hereafter, we call the chevron pattern in Fig. 3(a) DMC. The existence of spatially-periodic defect lines between alternating zig and zag rolls distinguishes DMC from DFC. DMC shows always spatiotemporal dynamics accompanied with defect motions [19,22].

Let us define $\lambda_1$ as the short wavelength for the striated rolls, and $\lambda_2$ as the long wavelength for the chevron bands, as illustrated in Fig. 3(b), similarly to Ref. [5]. We have measured the two wavelengths $\lambda_1$ and $\lambda_2$ in the DMC and DFC at $\varepsilon=0.1$, where $\varepsilon$ is a normalized voltage, i.e., $\varepsilon=(V^2-V_c^2)/V_c^2$. Figure 4 shows the dependence of $\lambda_1$ and $\lambda_2$ on the frequency $f$. There are two characteristic frequencies $f_L\simeq1450$ Hz [22], called the Lifshitz frequency (see, e.g., Ref. [15]), and $f_w\simeq3150$ Hz. First, the short wavelength $\lambda_1$ decreases continuously with increasing $f(<f_c)$. This frequency dependence of $\lambda_1(f<f_w)$ shows a qualitative

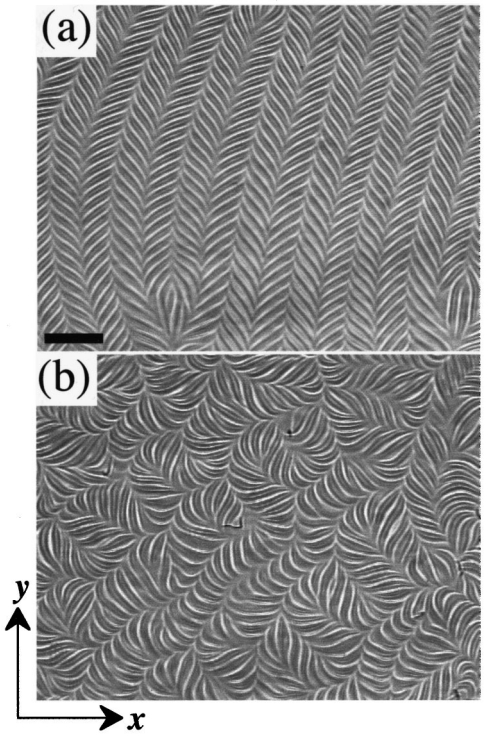


FIG. 2. One typical chevron (DFC) for $f>f_w$ in the conduction regime. (a) A spatially double-periodic chevron pattern at $V=149.40$ V and $f=3900$ Hz ($>f_w\simeq3150$ Hz), which was suddenly applied from the homogeneous Fréedericksz state ($V_F\simeq3.92$ V). (b) A spatiotemporally chaotic pattern with local chevron structures, which was obtained from (a) after waiting 1 h. The length of the scale bar in (a) is 200 $\mu$m.

agreement with that of $\lambda_c(f)$ at $\varepsilon=0$ in a previous paper [7]. Here $\lambda_1$ depends weakly on $f$ for $f<f_L$, while it depends strongly on $f$ for $f>f_L$. $\lambda_1$ is roughly of order $d$, the sample thickness ($d\leqslant\lambda_1\leqslant2d$). It is distinguishable from $\lambda_1\ll d$ for chevrons in the dielectric regime. Second, the long wavelength $\lambda_2(f)$ shows a quite different frequency dependence below and above $f_w$. For $f>f_w$ (DFC), $\lambda_2$ increases continuously with decreasing $f$ and diverges at $f_w$. The dependence $\lambda_2\sim(f-f_w)^{-1/4}$ for DFC is determined by the least-square regression. Here $f_w=3152$ Hz was determined by extrapolation. For $f<f_w$ (DMC), on the other hand, $\lambda_2$ increases continuously with decreasing $f$ and diverges at $f^*$ proportionally to $(f-f^*)^{-1/2}$, where $f^*=1842$ Hz. Since $f^*>f_L$, one finds no chevrons in the oblique-roll region ($f<f_L$). The fitting function for $\lambda_2$ is given by

$$\lambda_2(f)=\xi_1\left(\frac{f_w}{f-f_w}\right)^{1/4} \tag{1}$$

for DFC, and for DMC

$$\lambda_2(f)=\xi_2\left(\frac{f^*}{f-f^*}\right)^{1/2}, \tag{2}$$

where $\xi_1$ and $\xi_2$ are certain characteristic lengths 152 $\mu$m and 408 $\mu$m, respectively. Considering the different frequency dependence and the characteristics of the patterns below and above $f_w$, the mechanism of the DFC is clearly different from that of the DMC.

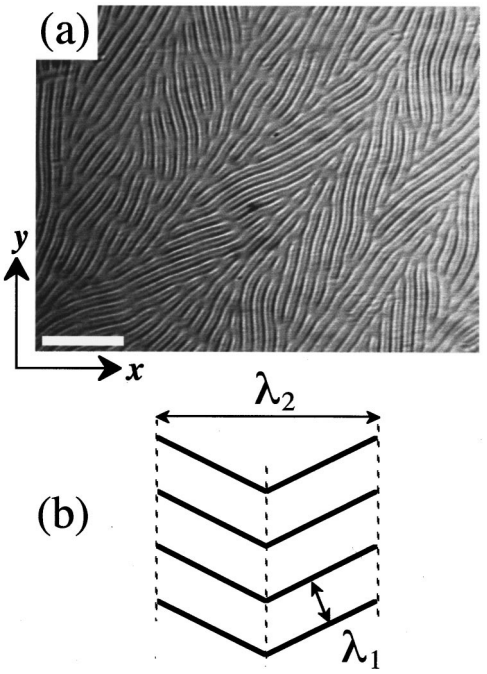


FIG. 3. The other typical chevron (DMC) for $f<f_w$ in the conduction regime. (a) A spatially double-periodic chevron pattern at $V=15.82$ V and $f=2000$ Hz ($<f_w\simeq 3150$ Hz), which is suddenly increased from the homogeneous Fréedericksz state ($V_F \simeq 3.92$ V). Unlike the DFC, the DMC has periodic defect lines between alternating zig and zag rolls. The DMC has always changed temporally and spatially with defect motions. (b) Illustration of the chevron shows two different spatial wavelengths, $\lambda_1$ and $\lambda_2$. The length of the scale bar is 400 $\mu$m.

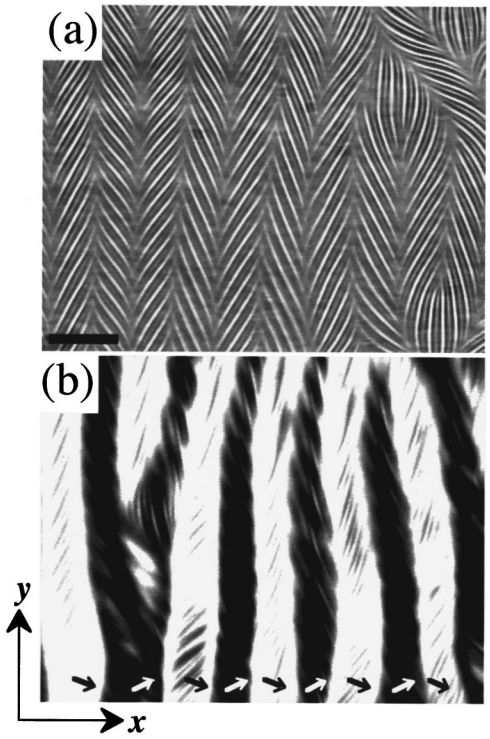


FIG. 5. Determination of the **C** director in the DFC ($V=147.7$ V and $f=3900$ Hz$>f_w$), (a) with no crossed polarizer set, and (b) under a crossed polarizer set with a 20° counterclockwise rotation to the $x$ axis. The **C**-director structure for the DFC can be determined from the direction and amplitude of the rotation of the crossed polarizer set. The **C**-director structure is depicted as thin arrows in (b). The length of the scale bar in (a) is 200 $\mu$m.

In the homeotropic case, one can directly monitor the **C** director under a crossed polarizer set [16,23]. The **C**-director field in the $xy$ plane has been carefully observed in both the DMC and DFC. Let us begin with the DFC at $V=147.7$ and $f=3900$ Hz($>f_w$), as shown in Fig. 5. A crossed polarizer set was inserted and rotated around the $z$ axis in order to determine the **C** director. The **C** director in the DFC is marked with thin arrows in Fig. 5(b). It should be noted that the optical intensity becomes minimal at regions where the **C** director is parallel to a polarizer [11,12]. The alternating zig and zag rolls are roughly normal to the corresponding **C** directors. In this frequency region ($f>f_w$), the DFC ($V>V_c$), formed from a *prewavy* pattern [33] ($V<V_c$) as the voltage was increased. Figure 6 shows the prewavy pattern at $V=75.56$ V($V<V_c=83.89$ V at $f=3500$ Hz), and the DFC at $V=88.88$ V($V>V_c$) under a crossed polarizer set. The prewavy pattern is never observed without a crossed polarizer set. The occurrence of the convection rolls (chevrons) is clearly related to a periodic **C**-director structure, which leads to the periodic optical contrast shown in Fig. 6(b). The chevron bands are closely correlated to the width of the stripes in the prewavy pattern. It is obvious that the prewavy pattern ($V<V_c$) is responsible for the long wavelength $\lambda_2$ of the DFC ($V>V_c$). The prewavy pattern originated from an elastic deformation of the director field. With the aid of a crossed polarizer set, the threshold voltage $V_w$ for the prewavy patterns was determined as shown in Fig. 7 [33]. It is found below $V_c$ in the frequency range $f>f_w$. Thus for $f>f_w$, one finds a sequence of bifurcations: Fréedericksz state → prewavy pattern → DFC with increasing voltage $V$. In particular, the prewavy pattern spontaneously changes into a sinusoidal wavy pattern, initiating a disclination [the arrow in Fig. 8(a), which also indicates the propa-

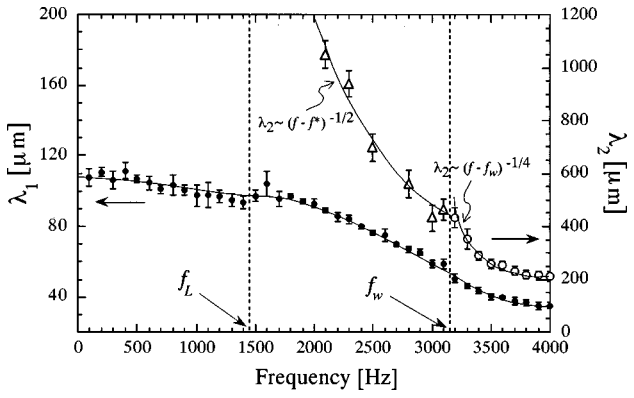


FIG. 4. Spatial structures for the DMC and DFC in the conduction regime for sample 3. There are two characteristic frequencies $f_L\simeq 1450$ Hz, the so-called Lifshitz frequency, and $f_w \simeq 3150$ Hz. Two wavelengths, $\lambda_1$ (solid circles) and $\lambda_2$ (open triangle: DMC; open circles: DFC), in chevrons have been measured at fixed control parameters $\varepsilon=0.1$ and $H_x=0$. The dependence of $\lambda_1$ on frequency $f$ is roughly continuous. The long wavelength $\lambda_2(f)$ shows the different frequency dependence below and above $f_w$. See text for details.

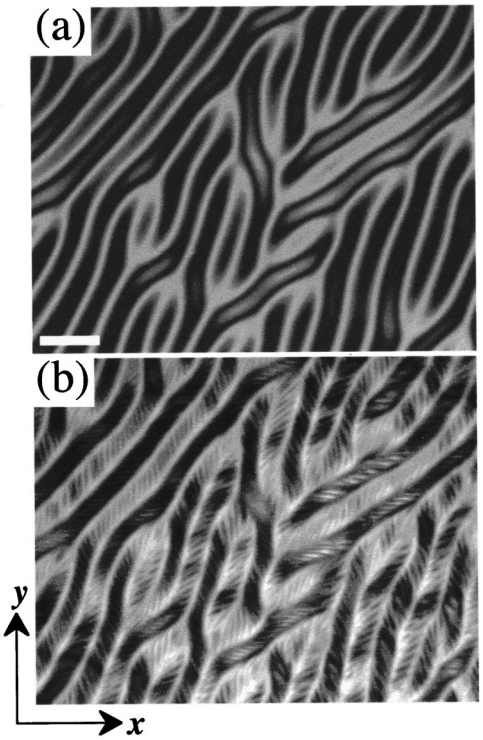


FIG. 6. Patterns below and above $V_c(=83.89\ \text{V})$ at $f=3500$ Hz $(>f_w)$. (a) The prewavy pattern at $V=75.56$ V between $V_w(=52.49\ \text{V})$ and $V_c$. (b) DFC at $V=88.88$ V above $V_c$. Here $V_w$ is the threshold for the prewavy pattern. These patterns were observed under a crossed polarizer set with a 20° counterclockwise rotation to the $x$ axis. The prewavy pattern is never observed without a crossed polarizer set. The width of the stripes in the prewavy pattern equals $\lambda_2/2$ for the DFC. The length of the scale bar in (a) is 200 $\mu$m.

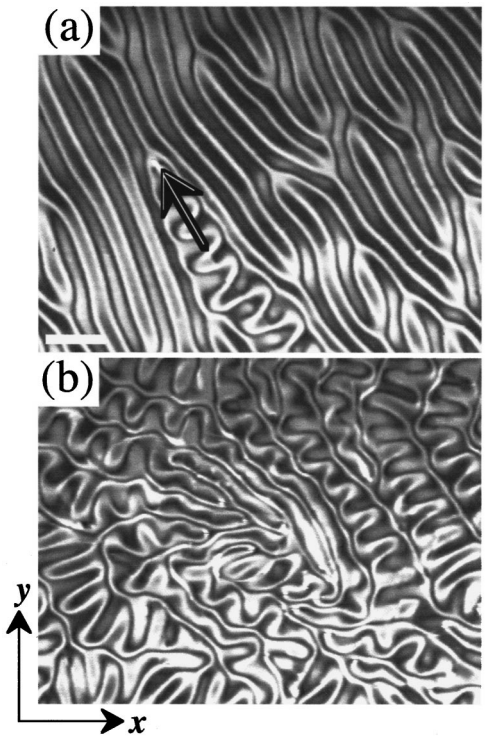


FIG. 8. Pattern change from the prewavy pattern to a propagating spiral pattern at $V=163.4$ V and $f=570$ Hz ($f_w\simeq 550$ Hz and $V_w=143.72$ V for sample 2). (a) At 5 min after forming a prewavy pattern as in Fig. 7(a). (b) At 30 min after forming the prewavy pattern. These patterns are never observed without a crossed polarizer set. Due to the triggering of a disclination [the arrow in (a)], the prewavy pattern eventually evolves into a propagating spiral pattern (b). The arrow in (a) also indicates a propagating direction. The length of the scale bar in (a) is 200 $\mu$m.

gating direction of the disclination]. The wavy pattern eventually evolves into a propagating spiral pattern shown in Fig. 8(b) [32,37,33]. A detailed study of the prewavy pattern and its evolution into the spiral pattern is now in progress.

Next the **C**-director field in the DMC ($f_L<f=2000$ Hz $<f_w$) was investigated. With the aid of the magnetic field $H_x=400$ G, which stabilizes the **C** director toward the $x$ axis, a sequent bifurcation to the DMC was observed with increasing voltage $V$. Figure 9(a) shows the Williams domains observed at $\varepsilon=0.05$. They turned out to be abnormal rolls ($\mathbf{C}\nparallel\mathbf{q}$) bifurcated from normal rolls ($\mathbf{C}\|\mathbf{q}$). (See Ref. [22] for the details about the threshold of abnormal rolls as a function of $H_x$.) Increasing $\varepsilon$ to 0.1, the abnormal rolls evolve into a spatiotemporally chaotic pattern with defect motions (i.e., the so-called defect chaos), as shown in Fig. 9(b). As the crossed polarizer set is rotated with respect to the $x$ axis ($\|\mathbf{H}$) at the same value $\varepsilon=0.1$, the bands of the DMC show alternating optical contrast, as shown in Fig. 9(c). Jumping from $\varepsilon=0.1$ to 0.2, the ordered DMC with periodic defect lines is observed as shown in Fig. 9(d). The **C** director determined from our measurements is given as thin arrows in Figs. 9(c) and 9(d). Similarly to the DFC, the alternating zig and zag rolls are roughly normal to the corresponding **C** directors. There exists no macroscopic pattern in the background such as the prewavy pattern for the DFC. Nevertheless, what determines the long wavelength $\lambda_2$ in the DMC? The defects may possibly play a role in determining $\lambda_2$ for the DMC [39].

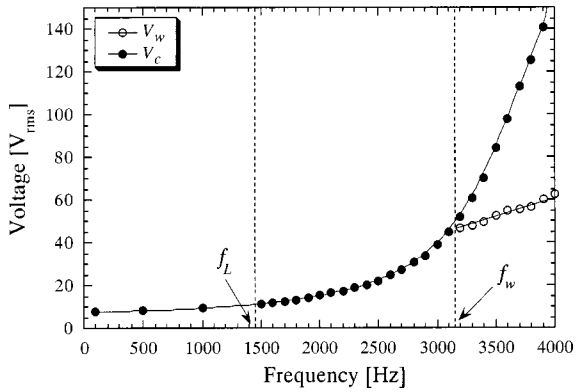


FIG. 7. Threshold $V_w$ for the prewavy pattern in sample 3. For $f>f_w$, $V_w$ (open circles) indicates the threshold voltage for the prewavy pattern, while $V_c$ (solid circles) indicates the critical voltage for the convection.

### C. Discussion

Since the alternating zig and zag rolls in the DMC and DFC result from the in-plane rotation of the **C** director, the obliqueness of the zig and zag rolls is determined from the

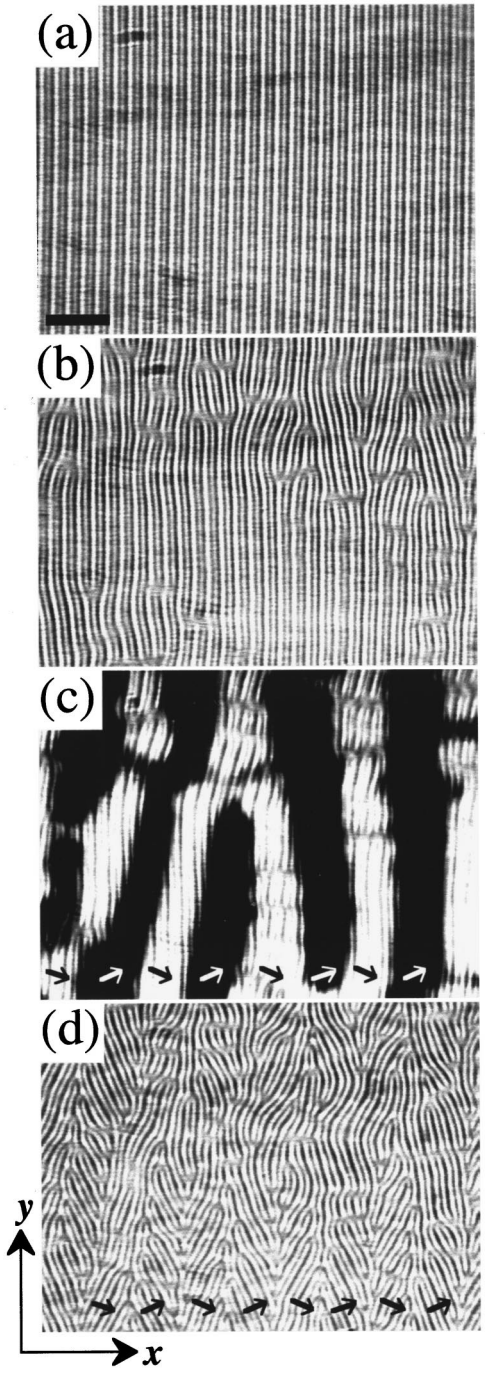


FIG. 9. Pattern evolution from abnormal rolls to the DMC ($f = 2000$ Hz$< f_w$). In a constant magnetic field $H_x = 400$ G, the pattern evolves from (a) to (d) with increasing the control parameter $\varepsilon$. (a) Abnormal rolls at $\varepsilon = 0.05$ (under no crossed polarizer set). (b) A spatiotemporal chaotic pattern with defect motions at $\varepsilon = 0.1$ (under no crossed polarizer set). (c) A spatiotemporal chaotic pattern with chevron bands at $\varepsilon = 0.1$ [under a crossed polarizer set with a 20° counterclockwise rotation to the $x$ axis ($\|\mathbf{H}$)], which was obtained from (b) after several minutes. (d) DMC at $\varepsilon = 0.2$ (under no crossed polarizer set). The abnormal rolls (a) ($\mathbf{C} \nparallel \mathbf{q}$) were bifurcated from normal rolls ($\mathbf{C} \| \mathbf{q}$). The **C**-director structure is depicted as thin arrows in (c) and (d). The length of the scale bar in (a) is 400 $\mu$m.

corresponding in-plane rotation. As to responsibility for the in-plane rotation, the prewavy instability for DFC can be safely distinguished from the abnormal roll instability for the DMC. That is, the former is not accompanied by convective flows, whereas the latter bifurcates from convective normal rolls. The prewavy instability observed in the present study thus is different from that due to the electrohydodynamic instabilities [28,29,43]. Past reports mentioned that the threshold line below $V_c$ was due to the inertia mode [29,42,43] or the isotropic mode [28]. Based on our experimental observation, since the prewavy instability has no steady flow [44], it is clearly distinguished from both modes which must have a steady flow. However, a periodic distribution of the director in the $xy$ plane [29,43,44] is similar to the prewavy instability. The details of this prewavy instability will be reported soon.

The mechanisms which lead to spatial periodicity on a length scale of $\lambda_2$ in the DMC and one in the DFC are not perfectly understood as yet. In the case of the DMC, the chevron pattern with alternating zig and zag rolls always appears via an instability of the abnormal roll. Below a critical voltage $V_{DMC}$ for the DMC, abnormal rolls are still stripe rolls, in spite of their finite in-plane rotation of the **C** director. With increasing voltage, the generated defects play a role in the formation of zig and zag rolls for the DMC. Thus the formation of a DMC may be considered as an example of the self-assembling phenomena of defects. Recently, Rossberg and Kramer proposed reaction-diffusion equations to qualitatively understand the DMC [39]. In their model, the topological charge density (i.e., defect density) $\rho$ and the **C**-director modulation $\partial_x \varphi$ play roles as an inhibitor and an activator, respectively. Thus a Turing pattern can be realized when the diffusion of the activator is slower than that of the inhibitor. This model describes the formation of a DMC out of defect chaos with an increase of a control parameter $h^2 \propto H^2/\varepsilon$ [38] similarly to Fig. 9 in the present study, as well as the appearance of a long wavelength $\lambda_2$. In the case of a DFC, on the other hand, the prewavy pattern may allow a length scale of $\lambda_2$ owing to a secondary twist-Fréedericksz transition. The flexoelectric effect has to be considered as a candidate responsible for the prewavy pattern.

Recently, Sakaguchi showed chevron patterns with alternating zig and zag rolls along the $x$ axis by numerical simulations using an anisotropic complex Swift-Hohenberg equation [40]. There are periodic sinks and sources of traveling waves which form their lines. The traveling zig and zag rolls (in a snapshot) look similar to the DFC. However, no argument is given as to in which sense the theoretical model might be related to EC.

In addition, the sequence of bifurcations from normal rolls to our DMC are quite similar to the experimental results in the dielectric regime in the planar case [31,33], although both systems are certainly different from each other. In the planar case with highly conductive samples, DFC's (slightly below $f_c$) as well as conventional dielectric chevrons (above $f_c$) were found (see, e.g., Ref. [29]).

## III. CONCLUSION

We have found three types of chevrons in a homeotropically aligned liquid crystal by varying the electrical conductiv-

TABLE I. Classification of chevrons found in the homeotropic system. Chevrons A and B in Refs. [33,34] were only classified through the difference of the short wavelength $\lambda_1$.

| Classification | Chevron A | | Chevron B |
|---|---|---|---|
| | Defect-mediated chevron (DMC) | Defect-free chevron (DFC) | Dielectric chevron |
| frequency | $f<f_w$ | $f_w<f<f_c$ | $f>f_c$ |
| $\lambda_1$ | $\lesssim 2d$ | $<d$ | $\ll d$ |
| $\lambda_2$ | $\sim \frac{1}{(f-f^*)^{1/2}}$ | $\sim \frac{1}{(f-f_w)^{1/4}}$ | ? |
| defects | existence | no existence | existence |
| pattern below $V_c$ | no existence | prewavy pattern | prewavy pattern |

ity. In the high-frequency dielectric regime ($f>f_c$) the chevrons are of the conventional type characterized by a very short wavelength ($\lambda_1 \ll d$). In the conduction regime ($f<f_c$) two different types of chevrons are observed in samples with high conductivity, that is, the DMC and DFC below and above a characteristic frequency $f_w$, respectively. In contrast to the conventional dielectric chevrons, the wavelength $\lambda_1$ of the DMC and DFC is of order $d$. The DFC is characterized by alternating zig and zag rolls with corresponding periodic rotations of the **C** director, whereas the DMC has periodic defect lines between the alternating zig and zag rolls.

We have clearly demonstrated that the prewavy pattern ($f>f_w$) appearing below $V_c$ triggers the DFC above $V_c$. Thus we conclude that the DFC ($f>f_w$) results from one sequence of bifurcations (Fréedericksz transition → prewavy pattern → DFC) with increasing voltage. With the aid of a weak magnetic field and a crossed polarizer set, we have also found the other sequence for the DMC ($f<f_w$) (normal rolls → abnormal rolls → defect chaos → DMC) with increasing voltage. We propose that both the abnormal-roll mechanism and defects together lead to the DMC. It is obvious that there are different mechanisms for formation of chevrons below and above $f_w$. Obviously, the wavelength $\lambda_2(f)$ shows different frequency dependences such as $\lambda_2(f)\sim(f-f^*)^{-1/2}$ for the DMC and $\lambda_2(f)\sim(f-f_w)^{-1/4}$ for the DFC. Thus we have classified all the chevrons found in the homeotropic system in Table I.

As mentioned in Sec. I, the free-rotational mode in the homeotropic system is crucial for the formation of chevrons in the conduction regime. In both the DMC and DFC, the chevrons have always shown a periodic **C**-director structure in the $xy$ plane, although their individual features and driving mechanisms are clearly different. Therefore, we finally conclude that the in-plane rotational mode (due to either the abnormal roll instability or the prewavy instability) is necessary to form chevron patterns. The angle of the in-plane rotation of the **C** director determines the obliqueness of alternating zig and zag rolls, which are roughly normal to the corresponding **C** directors.

## ACKNOWLEDGMENTS

The authors thank W. Pesch for valuable discussions. This work was partly supported by a Grant-in-Aid for Scientific Research from the Ministry of Education, Science, Sports and Culture in Japan (Nos. 08454107 and 10440117).

[1] M.C. Cross and P.C. Hohenberg, Rev. Mod. Phys. **65**, 851 (1993).
[2] L. Kramer and W. Pesch, Annu. Rev. Fluid Mech. **27**, 515 (1995).
[3] Orsay Liquid Crystal Group, Mol. Cryst. Liq. Cryst. **12**, 251 (1971).
[4] I. W. Smith, Y. Galerne, S. T. Lagerwall, E. Dubois-Violette, and G. Durand, J. Phys. (Paris), Colloq. **C1-237** (1975).
[5] S. Kai and W. Zimmermann, Suppl. Prog. Theor. Phys. **99**, 458 (1989).
[6] L. Kramer, A. Hertrich and A. Pesch, *Pattern Formation in Complex Dissipative Systems*, edited by S. Kai (World Scientific, Singapore, 1992), p. 238.
[7] H. Richter, N. Klöpper, A. Hertrich, and A. Buka, Europhys. Lett. **30**, 37 (1995).
[8] W. Pesch and U. Behn, in *Evolution of Spontaneous Structures in Dissipative Continuous Systems*, edited by F. H. Busse and S. C. Mueller (Springer, New York, 1998).
[9] E.F. Carr, Mol. Cryst. Liq. Cryst. **7**, 256 (1969).
[10] W. Helfrich, J. Chem. Phys. **51**, 4092 (1969).
[11] L. M. Blinov, *Electro-optical and Magneto-optical Properties of Liquid Crystals* [The Universities Press (Belfast) Ltd., Northern Ireland, 1983].
[12] P. G. de Gennes and J. Prost, *The Physics of Liquid Crystals*, 2nd ed. (Oxford University Press, New York, 1993).
[13] E. Plaut, W. Decker, A.G. Rossberg, L. Kramer, W. Pesch, A. Belaidi, and R. Ribotta, Phys. Rev. Lett. **79**, 2367 (1997).
[14] E. Plaut and W. Pesch, Phys. Rev. E **59**, 1747 (1999).
[15] A. Hertrich, W. Decker, W. Pesch, and L. Kramer, J. Phys. II **2**, 1915 (1992).
[16] H. Richter, A. Buka, and I. Rehberg, Mol. Cryst. Liq. Cryst. **251**, 181 (1994); Phys. Rev. E **51**, 5886 (1995).
[17] A.G. Rossberg, A. Hertrich, L. Kramer, and W. Pesch, Phys. Rev. Lett. **76**, 4729 (1996).
[18] S. Kai, K. Hayashi, and Y. Hidaka, J. Phys. Chem. **100**, 19007 (1996).

[19] Y. Hidaka, J.-H. Huh, K. Hayashi, M.I. Tribelsky, and S. Kai, Phys. Rev. E **56**, R6256 (1997); Y. Hidaka, J.-H. Huh, K. Hayashi, M.I. Tribelsky, and S. Kai, J. Phys. Soc. Jpn. **66**, 3329 (1997).
[20] J.-H. Huh, Y. Hidaka, and S. Kai, J. Phys. Soc. Jpn. **67**, 1948 (1998).
[21] P. Toth, A. Buka, J. Peinke, and L. Kramer, Phys. Rev. E **58**, 1983 (1998).
[22] J.-H. Huh, Y. Hidaka, and S. Kai, J. Phys. Soc. Jpn. **68**, 1567 (1999).
[23] J.-H. Huh, Y. Hidaka, and S. Kai, Phys. Rev. E **58**, 7355 (1998).
[24] G. Heilmeier and W. Helfrich, Appl. Phys. Lett. **16**, 155 (1970).
[25] Y. Galerne, G. Durand, and M. Veyssie, Phys. Rev. A **58**, 484 (1972); Y. Galerne, G. Durand, M. Veyssie, and V. Pontikis, Phys. Lett. **38A**, 449 (1972).
[26] S. Kai, K. Yamaguchi, and K. Hirakawa, Jpn. J. Appl. Phys. **14**, 1653 (1975).
[27] N.V.S. Rao, P.R. Kishore, T.F.S. Raj, M.N. Avadhanlu, and C.R.K. Murty, Mol. Cryst. Liq. Cryst. **36**, 65 (1976).
[28] R. Ribotta and G. Durand, J. Phys. (Paris), Colloq. **C3-334**, (1979).
[29] A. N. Trufanov, L. M. Blinov, and M. I. Barnik, Zh. Éksp. Teor. Fiz. **78**, 622 (1980) [Sov. Phys. JETP **51**, 314 (1980)].
[30] H. Yamazaki, S. Kai, and K. Hirakawa, J. Phys. Soc. Jpn. **56**, 502 (1987).
[31] M. Scheuring, L. Kramer, and J. Peinke, Phys. Rev. E **58**, 2018 (1998).
[32] S. Kai and K. Hirakawa, Solid State Commun. **18**, 1573 (1976).
[33] S. Kai, Y. Adachi, and S. Nasuno, in *Spatio-Temporal Patterns*, edited by P. E. Cladis and P. Palffy-Muhoray (Addison-Wesley, Reading, MA, 1995), p. 313.
[34] S. Kai and K. Hirakawa, Mem. Fac. Kyushu Univ. **36**, 269 (1977).
[35] M.I. Barnik, L.M. Blinov, M.F. Grebenkin, and A.N. Trufanov, Mol. Cryst. Liq. Cryst. **37**, 47 (1976).
[36] W.R. Krigbaum and H.J. Lader, Mol. Cryst. Liq. Cryst. **62**, 87 (1980).
[37] K. Hirakawa and S. Kai, Mol. Cryst. Liq. Cryst. **40**, 261 (1977).
[38] A. G. Rossberg, Ph.D. thesis, University of Bayreuth, 1997.
[39] A.G. Rossberg and L. Kramer, Physica D **115**, 19 (1998).
[40] H. Sakaguchi, Phys. Rev. E **58**, 8021 (1998).
[41] E. Bodenschatz, W. Zimmermann, and L. Kramer, J. Phys. (France) **49**, 1875 (1988).
[42] L. M. Blinov and V. G. Chigrinov, *Electrooptic Effects in Liquid Crystal Materials* (Springer-Verlag, New York, 1994).
[43] L. Nasta, A. Lupu, and M. Giurgea, Mol. Cryst. Liq. Cryst. **71**, 65 (1981).
[44] P. Petrescu and M. Giurgea, Phys. Lett. **59A**, 41 (1976).